

# Miniaturized Microstrip Filter Design Using Active Learning Method

Payman REZAEI<sup>1,2</sup>, Majid TAYARANI<sup>1</sup>, Reinhard KNÖCHEL<sup>2</sup>

<sup>1</sup> Dept. of Electrical Engineering, Iran University of Science and Technology, Narmak, Tehran, 1684613114, Iran

<sup>2</sup> Microwave Group, Christian-Albrechts-University of Kiel, Kiel, 24143, Germany

pre@tf.uni-kiel.de, m\_tayarani@iust.ac.ir, rk@tf.uni-kiel.de

**Abstract.** *Relating coupling and external quality factor of a filter to the physical parameters of the structure which is the final step of any filter design is usually complicated due to geometrical complexities of the filter, or in the case of microstrip resonators due to the lack of the exact solution for the field distribution. Therefore, common approach is using time consuming full wave simulations. In this paper active learning method (ALM) which is a fuzzy-based modeling technique developed by a procedure algorithmically mimics the information-handling process of the human brain, is proposed to overcome this drawback. Modeling steps of an unknown function using ALM will be described using an illustrative example. Afterwards, the modeling approach will be implemented to model coupling factor between two coupled spiral resonators (SRs) for two different coupling structures and external quality factor of the same resonator. Accuracy of the extracted surfaces is validated using two different criteria. Using the extracted surfaces; a four pole Chebychev bandpass filter was designed and fabricated. Good agreement between the measured response and simulation validated the accuracy of the extracted surfaces again. Comparing the fabricated SR filter with a square open loop resonator (SOLR) one demonstrates more than 70% of filter area reduction.*

## Keywords

Active learning method, coupling factor computation, external quality factor computation, soft computing techniques, spiral resonator.

## 1. Introduction

Due to the increasing complexity and variety of microwave structures, the number of design variables is on the rise. Although Maxwell's equations are satisfied in all electromagnetic structures, but still a lot of different structures could be found without any analytical solution which motivated designers using numerical methods. Time consuming process of these full wave simulations prompted designers to the use of circuit-based models which are not precise as EM-based models are, but they are fast enough.

The main idea of this paper is to introduce a method for microwave structure modeling with different modeling parameters which benefits from EM-based modeling techniques accuracy, circuit-based modeling fastness but does not suffer from the huge amount of calculations. In this regard, the ability of soft computing techniques in modeling complicated problems may provide such a useful facility. Among the soft computing techniques the ability of fuzzy inference method in solving complicated electromagnetic problems such as; microwave filter tuning [1], [2], EMC problems [3], resonant frequency computation [4], [5], also antenna modeling [6], [7] has been proved in various publications. Artificial neural network (ANN), which is also a well-known soft computing technique, has been used recently in microwave filter design [8]. Although the modeling steps of these methods seem to be very similar to the human logical-thinking the amount and complexity of mathematics which is used, even in ordinary fuzzy-based modeling techniques [9], [10], is usually forgotten.

ALM which is a relatively new soft computing technique [11], [12] does not suffer from the mathematical complexity of fuzzy algorithms, time consuming training process of ANN-based techniques, also difficulty of the interpretation of the embedded knowledge in the trained ANNs. This method is similar to the way which human being looks at any phenomena, acquires data from it, extracts knowledge about the observed events and finally the decision he makes about the total system. In ALM, any multi-input single-output (MISO) system is supposed to be as the combination of some single-input single-output (SISO) one. Behavior of each SISO system which is a curve and a spread related to it is extracted by the ink drop spread (IDS) method versus the corresponding independent variables. Then using an appropriate combination rule of inference, the general behavior of the system is understood.

Considering the simplicity, interpretability, fastness and accuracy of the ALM method, in this paper a quite general ALM-based approach for coupling and external quality factor computation is proposed. The paper is organized as follows. Basic definitions of ALM, clarifying the modeling steps using an illustrative example and its

general formulation are described in section 2. Section 3 is devoted to the implementation of ALM for coupling and external quality factor modeling of SRs versus two and three important physical parameters respectively. In section 4 extracted coupling and external quality factor surfaces are implemented to design a four pole Chebychev SR filter, then comparison of the dimensions of the designed SR filter and an open loop resonator one illustrates the amount of miniaturization provided by the SR configurations. Finally, conclusions are presented in section 5.

## 2. ALM Definition

ALM is mainly characterized by its intuitive pattern-based processing, which is based on the hypothesis that humans interpret information in the form of pattern-like images rather than numerical or logical forms. Confronting any new experiment creates a new pattern in the brain. Therefore, each pattern represents a simple concept, and by the combination of these basic patterns, complicated subjects can be expressed and understood. Fig. 1 shows the flow diagram of the method. According to this flow diagram, ALM uses the following steps to model an unknown system or function versus the total number of independent variables that affect its behavior or output value.

- At first, sample data are gathered by any numerical method or measurement technique.
- In the second step which is usually called projection step, all the gathered data are projected on each  $x_i$ -y plane where  $x_i$  is the  $i$ th input variable and  $y$  stands for the output.
- In this step, we are trying to imagine that the system is composed of some SISO one. If the system was really a SISO one, the projected data would provide a narrow unique path, but because of the effect of other inputs, a spread is detectable around each narrow path. This spread shows the effect of other input variables on the corresponding  $x_i$ -y plane. It can be easily deduced that, the narrower this spread; the effects of other input parameters on the output computation are less.
- In the third step, the IDS algorithm is run for each initial data point in the corresponding  $x_i$ -y plane, to extract the behavior of each SISO system.

In the IDS method, we assume each data point in each  $x_i$ -y plane as a light source which has a cone shaped beam width. When the vertical distance from this point increases its pattern spreads and interferes with the pattern of other data points which are now other sources of light. Indeed these cones are three dimensional membership functions which show the degree of confidence to other points near data points. If the mixed patterns are plotted on the corresponding input-output plane in grayscale, a pattern will be constructed as shown in Fig. 2. The process of grayscale representation of the data in each  $x_i$ -y plane is called IDS.

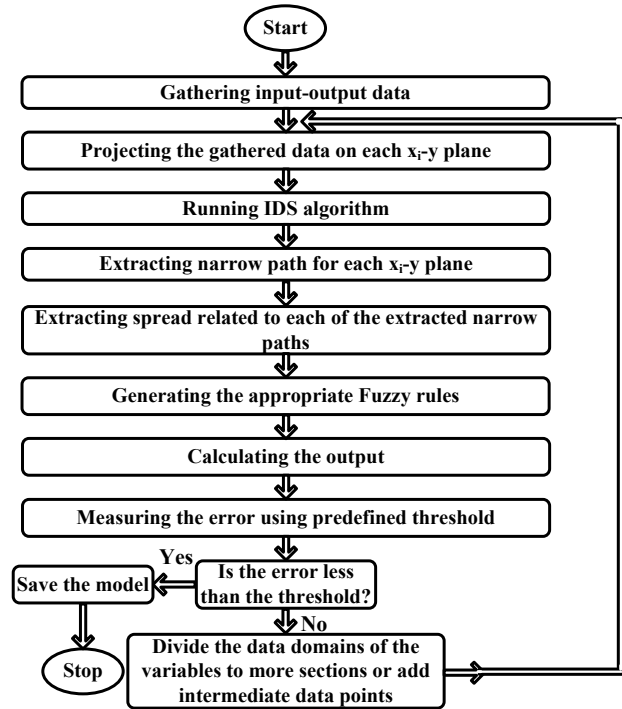


Fig. 1. Flow diagram of ALM for modeling an unknown function.

- In the fourth step, behavior of each SISO system is extracted from the IDS pattern using (1).

$$\psi(x) = \left\{ k \left| \sum_{y=y_{\min}}^k d(x, y) \approx \sum_{y=k}^{y_{\max}} d(x, y) \right. \right\} \quad (1)$$

where  $\psi(x)$  is the extracted narrow path for the input parameter  $x$ .  $d(a, b)$  is the value of darkness in point  $(a, b)$ . This value is 1 for the darkest points which are the most confident points in the plane and is 0 for the lightest ones.

- In the fifth step for each extracted narrow path, a spread is calculated using (2). This parameter indicates the effect of the corresponding input in overall system output.

$$\sigma(x) = \max\{y | d(x, y) > 0\} - \min\{y | d(x, y) > 0\} \quad (2)$$

- In the sixth step according to the number of divisions for each input variable, appropriate fuzzy rules of inference will be produced.

As an example if, for a two-input function, each input domain is divided into two sections there are four inference rules as follows.



Fig. 2. A typical IDS pattern.

$$\begin{aligned} R_{1k} &: \text{If } x_2 \text{ is } A_{2k}, \text{ then } y \text{ is } \psi_{1k}, k = 1, 2 \\ R_{2k} &: \text{If } x_1 \text{ is } A_{1k}, \text{ then } y \text{ is } \psi_{2k}, k = 1, 2 \end{aligned} \quad (3)$$

where  $\psi_{ij}$  is the  $j$ th narrow path for the  $i$ th input variable, and  $A_{ij}$  denotes the  $j$ th membership function for the  $i$ th input variable.

- Finally, the model output is obtained by aggregating the narrow paths. For a two-input function, with two divisions for each variable, model output is calculated as follows.

$$y \text{ is } \beta_{11}\psi_{11} \text{ or } \beta_{12}\psi_{12} \text{ or } \beta_{21}\psi_{21} \text{ or } \beta_{22}\psi_{22} \quad (4)$$

where  $\cup$  is the union operator and  $\beta_{ij}$  denotes the weight of the  $j$ th narrow path for the  $i$ th input variable. The value of  $\beta$  is determined from the spread and the degree of truth of the antecedent part in (3). It is calculated as follows.

$$\beta_{1k_1} = \frac{\omega_{1k_1} \times A_{2k_1}}{\omega_{11} \times A_{21} + \omega_{12} \times A_{22} + \omega_{21} \times A_{11} + \omega_{22} \times A_{12}},$$

$$\beta_{2k_2} = \frac{\omega_{2k_2} \times A_{1k_2}}{\omega_{11} \times A_{21} + \omega_{12} \times A_{22} + \omega_{21} \times A_{11} + \omega_{22} \times A_{12}}, \quad (5)$$

$$\omega_{ij} = 1/\sigma_{ij}, \quad i=1,2; \quad j=1,2; \quad k_1=1,2; \quad k_2=1,2$$

- In the eighth step, the output of the constructed model is compared with the original output by a predefined threshold error. If the model is not accurate enough, the input domains will be divided in more sections, and if it is necessary intermediate data points will be added to the previous ones. The active learning method is run again to reduce the error of the model.

### 2.1 A Two-Input Function Modeling by ALM

In order to explain the modeling process of ALM, we use a two-input function that has an input-output relationship as shown in Fig. 3(a). For the simplicity of explanation, each input domain is divided into two parts as shown in Fig. 3(b). Therefore, four SISO systems are generated, i.e., A, B, C, and D. In this figure,  $A_{ij}$  is the  $j$ th membership function for the  $i$ th input variable. Projected data of parts B and C on the corresponding  $x_i$ - $y$  plane are shown in Fig. 4.

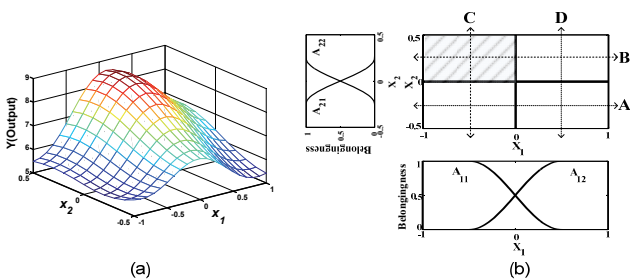


Fig. 3. (a) Input-output relationship of a two-input function and (b) input domains divisions and corresponding membership functions.

In order to extract the behavior of the system in the shaded area of Fig. 3(b), it is only necessary to consider  $x_1$  in the interval  $[-1 \ 0]$  of the part B and  $x_2$  in the interval  $[0 \ 0.5]$  of the part C. As it can be seen in Fig. 4, for the men-

tioned interval of  $x_2$  in the part C a wide spread is detectable, therefore, no information about the output can be elicited from this projected data. On the other hand, in the mentioned interval for the  $x_1$  in the part B there is a thin spread which means a high correlation between  $x_1$  and the output. Therefore, part B effectively elicits the system feature of the shaded area. In order to extract the behavior of the system in the total variation range of the inputs, all data of parts A to D should be utilized. For each of these parts, the related narrow path which explains the behavior of the corresponding SISO system, and, the related spread which explains the effect of other inputs on the extracted narrow path, are obtained using IDS algorithm as shown in Fig. 5.

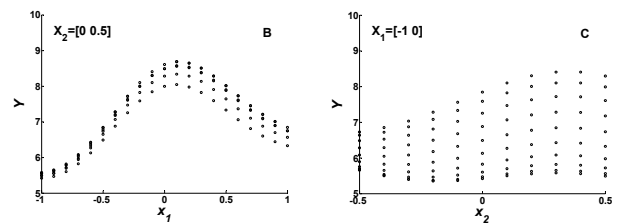


Fig. 4. Projected data on the corresponding  $x_i$ - $y$  plane for the parts B and C.

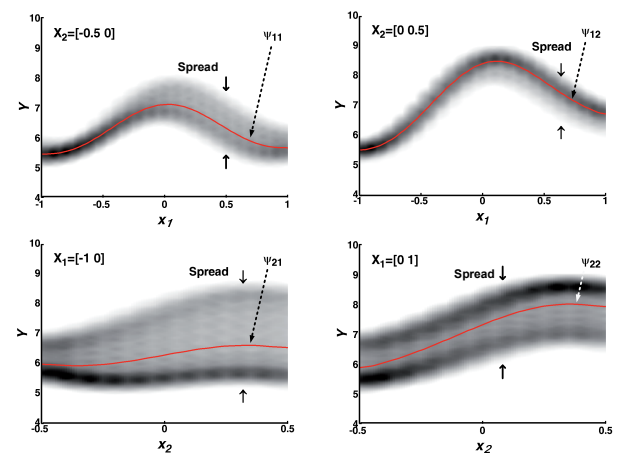


Fig. 5. IDS pattern of four SISO systems. Red curves are extracted narrow paths. Spreads, which are the width of the dark area in the  $y$  direction, are also visible in these figures.

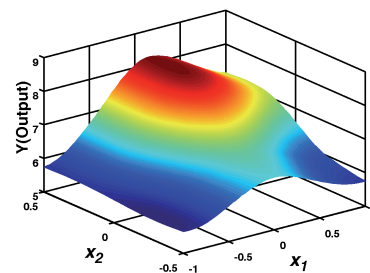


Fig. 6. Extracted input-output relationship.

Finally, using extracted narrow paths and spreads the output of the system is computed using (4) as shown in

Fig. 6. It should be mentioned that the utilized membership functions for this modeling have cosine form as follows.

$$\begin{cases} \frac{1}{2} \left( 1 + \cos \pi \left( \frac{x-a}{b-a} \right) \right) & \text{for } x : a \rightarrow b \\ \frac{1}{2} \left( 1 - \cos \pi \left( \frac{x-a}{b-a} \right) \right) & \text{for } x : a \rightarrow b \end{cases} \quad (6)$$

where  $x$  is variable.

### 2.2 ALM for Three-Input Systems

In this section, the ALM formulation for modeling of an unknown function with three independent variables which are referred to as  $x_1, x_2$  and  $x_3$  is described. Suppose each input domain is divided into  $m_1, m_2$  and  $m_3$  partitions respectively. Therefore, the number of IDS units is calculated as follows.

$$L = \sum_{i=1}^3 l_i, \quad l_i = \prod_{\substack{j=1 \\ j \neq i}}^3 m_j \quad (7)$$

where  $L$  is the total number of IDS units, and  $l_i$  denotes the number of IDS units for the input variable  $x_i$ .  $L$  also denotes the number of inference rules. Some of these inference rules are as shown in (8).

$$\begin{aligned} R_{11} : & \text{If } x_2 \text{ is } A_{21} \text{ and } x_3 \text{ is } A_{31}, \text{ then } y \text{ is } \psi_{11}, \\ & \vdots \\ R_{1l_1} : & \text{If } x_2 \text{ is } A_{2m_2} \text{ and } x_3 \text{ is } A_{3m_3}, \text{ then } y \text{ is } \psi_{1l_1}, \\ R_{21} : & \text{If } x_1 \text{ is } A_{11} \text{ and } x_3 \text{ is } A_{31}, \text{ then } y \text{ is } \psi_{21}, \\ & \vdots \\ R_{3l_3} : & \text{If } x_1 \text{ is } A_{1m_1} \text{ and } x_2 \text{ is } A_{2m_2}, \text{ then } y \text{ is } \psi_{3l_3}. \end{aligned} \quad (8)$$

Finally, all the extracted narrow paths, spreads, and membership functions are used for output model computation (9).

$$\begin{aligned} y & \text{ is } \beta_{11} \psi_{11} \text{ or } \dots \text{ or } \beta_{ik} \psi_{ik} \text{ or } \dots \text{ or } \beta_{3l_3} \psi_{3l_3}, \\ k & = 1, 2, \dots, l_i, \quad i = 1, 2, 3 \end{aligned} \quad (9)$$

where  $\beta_{ik}$  is calculated as follows.

$$\beta_{ik} = \frac{\omega_{ik} \times \Gamma_{ik}}{\sum_{i=1}^3 \sum_{k=1}^{l_i} \omega_{ik} \times \Gamma_{ik}}. \quad (10)$$

In this equation  $\Gamma_{ik}$  is calculated using (11).

$$\begin{aligned} \Gamma_{11} & = A_{21} \wedge A_{31}, \dots, \Gamma_{1l_1} = A_{2m_2} \wedge A_{3m_3}, \\ \Gamma_{21} & = A_{11} \wedge A_{31}, \dots, \Gamma_{3l_3} = A_{1m_1} \wedge A_{2m_2} \end{aligned} \quad (11)$$

where  $\wedge$  is the intersection operator of the fuzzy sets.

It should be emphasized that the flow diagram of Fig. 1 is valid for ALM modeling of an unknown function with any required number of input variables.

## 3. Coupling and External Quality Factor Modeling Using ALM

In the following subsection, coupling and external quality factor are briefly described, and some references are addressed concerning common approach to open loop filter design using coupling factor matrix. In the next subsection, ALM is implemented for modeling these two factors for a distinct SR. Extracted ALM-based coupling and external quality factor surfaces are utilized in section 4 as a filter design tool.

### 3.1 Brief Definition of Coupling and External Quality Factor

Coupling factor, which is the most important quantity in designing any narrow band filter, can be calculated using the following equation.

$$K = \frac{f_e^2 - f_m^2}{f_e^2 + f_m^2} \quad (12)$$

where  $f_e$  and  $f_m$  are even and odd resonant frequencies of the two coupled resonators, which occur at the frequencies where  $S_{11}$  has its minimum value [13]. Fig. 7(a) and 7(b) show two different structures of the coupled SRs.

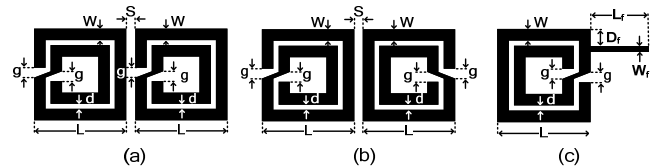


Fig. 7. Coupled SRs, (a) mixed coupling and (b) magnetic coupling. (c) Typical tapped-line feeding structure for a SR.

Another important quantity in the filter design is external quality factor ( $Q_{ext}$ ). This factor can be described as the coupling of a resonator to an external circuit. For every resonant circuit,  $Q_{ext}$  can be computed by the aid of unloaded quality factor ( $Q_U$ ) and loaded quality factor ( $Q_L$ ) as it is shown in (13) [14].

$$\frac{1}{Q_{ext}} = \frac{1}{Q_L} - \frac{1}{Q_U}. \quad (13)$$

A typical tapped line feeding structure which is used to excite a SR has been shown in Fig. 7(c).  $Q_{ext}$  of this structure is modeled in the following subsection.

Early after the first introduction of SOLRs in [15], different coupling structures and a filter design example using coupling coefficient approach was described in [13]. The same process has been applied to other kinds of open loop resonators such as triangular [16], pentagonal [17], hexagonal [18], and even SRs. The final step of the approach, which has been described in [13] and implemented in [16]-[18], is devoted to the calculation of required coupling factors through the use of time consuming

full wave simulators. In these references, the problem of external quality factor computation for all kinds of open loop resonators was neglected. To avoid this time consuming process of coupling factor computation and, to introduce an approach for determination of the feed line physical parameters according to the required external quality factor use of ALM is proposed.

### 3.2 Modeling Steps

In this subsection, the effect of substrate height ( $h$ ) in the range of [0.5 mm 2 mm] and spacing between resonators ( $S$ ) in the range of [0.3 mm 3.3 mm] on the mixed and magnetic coupling factors (Fig. 7(a) and 7(b)) is modeled using the discussed modeling technique. Afterwards, the effect of feed line length ( $L_f$ ), feed line position ( $D_f$ ), and feed line width ( $W_f$ ) on the  $Q_{ext}$  is modeled for the structure shown in Fig. 7(c). In this modeling  $L_f$ ,  $D_f$ , and  $W_f$  are within the range of [2 mm 12 mm], [0 2 mm], and [0.2 mm 0.8 mm] respectively. In order to clarify the modeling steps a distinct SR with the following dimensions is used;  $W = 0.7$  mm,  $g = 0.6$  mm,  $L = 5.6$  mm, and  $d = 0.3$  m. Selected substrate permittivity for these modelings is 9.8. In the  $Q_{ext}$  modeling, the substrate height is selected to be 1.27 mm.

The following steps have been carried out to construct the ALM-based coupling and external quality factor surfaces:

- Mixed and magnetic coupling factors have been calculated using Ansoft HFSS-13 for 36 points within the variation range of the modeling parameters, i.e.,  $h$  and  $S$ . These are the required initial input data for the construction of coupling factor model. In the same way,  $Q_{ext}$  of Fig. 7(c) has been calculated using Ansoft HFSS-13 for 120 data points within the variation range of  $W_f$ ,  $L_f$ , and  $D_f$ . These data points are the required initial inputs for the construction of  $Q_{ext}$  model.
- Concerning the mixed and magnetic coupling factor modeling, the variation range of  $h$  and  $S$  has been divided into 3 and 8 sections respectively. Concerning the  $Q_{ext}$  modeling, the variation range of  $W_f$ ,  $L_f$ , and  $D_f$  has been divided into 4, 5, and 3 sections respectively.
- Initial data of each section have been projected on the corresponding  $x$ - $y$  plane, and related IDS patterns have been constructed for each SISO system.
- Using the constructed IDS patterns, the narrow path and spread of different SISO systems have been computed by the aid of (1) and (2) respectively.
- Finally, the model output has been calculated using (9). In this calculation extracted narrow paths and spreads and the cosine form membership functions (6), which are allocated to each of the independent variables according to the number of divisions, have been used.

Fig. 8 shows the extracted ALM-based coupling factor surfaces for the mixed and magnetically coupled SRs. According to the number of independent variables for the  $Q_{ext}$  modeling which are three ones, we need a four dimensional space for representation of the results in one figure, which is not possible. In this regard, Fig. 9(a) - 9(c) show the extracted  $Q_{ext}$  surfaces versus two of the modeling parameters. In each of these figures, one of the independent variables has been set to three different values, and the other ones sweep their own range of variations.

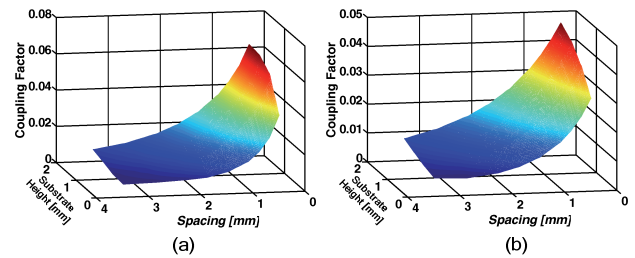


Fig. 8. ALM-based extracted coupling surfaces for the coupled SRs, (a) mixed coupling, (b) magnetic coupling.

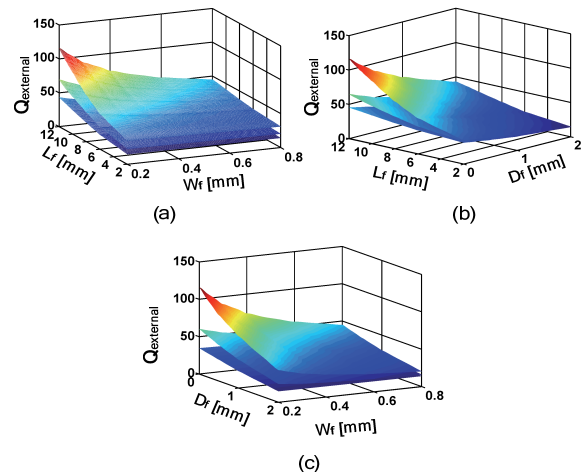


Fig. 9. Extracted  $Q_{ext}$  for the structure of Fig 7(c), (a)  $D_f=0$  (top),  $D_f=1$  mm (middle),  $D_f=2$  mm (bottom), (b)  $W_f=0.2$  mm (top),  $W_f=0.5$  mm (middle),  $W_f=0.8$  mm (bottom), and (c)  $L_f=12$  mm (top),  $L_f=7$  mm (middle),  $L_f=2$  mm (bottom).

Resolution of the extracted coupling factor surfaces is 0.005 mm for each of the independent variables. For the extracted  $Q_{ext}$  surfaces, resolution is equal to 0.05 mm, 0.002 mm, and 0.002 mm, for  $L_f$ ,  $D_f$ , and  $W_f$  respectively. Considering the above resolution each of the mixed or magnetic coupling surfaces consists of  $601 \times 301$  points and the extracted quality factor consists of  $241 \times 301 \times 901$  points. ALM needs a few minutes, for modeling each of these mixed and magnetic coupling surfaces, and less than half an hour for modeling external quality factor versus its three independent variables, while Ansoft HFSS-13 needs 9 minutes for each point of these coupling factor surfaces, and 3 minutes for each point of the external quality factor surfaces. In other words, Ansoft HFSS-13 needs more than 3 years for computing each of the coupling factor surfaces

and 373 years for computing external quality factor data. This comparison clearly shows the ability of the ALM method in providing a vanishingly fast modeling tool, with a high resolution of the extracted data for coupling and external quality factor computations within a wide variation range of the independent variables which seems almost impossible by the full wave approach. It should be emphasized that the modeling approach and modeling simplicity remains unchanged when the number of modeling variables increases because, in this modeling technique, every complex system is broken down into its simpler aspects, to acquire useful information in a more comprehensible form.

In order to verify the model accuracy, the error between the target function (full-wave-based extracted data) and the constructed model (ALM-based extracted data) was measured using two different criteria, i.e., the fraction of variance unexplained (FVU) and correlation coefficient (CC), which are defined as follows.

$$FVU = \frac{\sum_{l=1}^N (y_l - \hat{y}_l)}{\sum_{l=1}^N \left( y_l - \frac{1}{N} \sum_{l=1}^N y_l \right)^2}, \quad (14)$$

$$CC = \frac{\sum_{l=1}^N \left( y_l - \frac{1}{N} \sum_{l=1}^N y_l \right) \left( \hat{y}_l - \frac{1}{N} \sum_{l=1}^N \hat{y}_l \right)}{\sqrt{\left( \sum_{l=1}^N \left( y_l - \frac{1}{N} \sum_{l=1}^N y_l \right)^2 \right) \left( \sum_{l=1}^N \left( \hat{y}_l - \frac{1}{N} \sum_{l=1}^N \hat{y}_l \right)^2 \right)}} \quad (15)$$

where  $y_l$  and  $\hat{y}_l$  denote the  $l$ th data point of the output vector and the constructed model respectively.  $N$  is the total number of the output vector.

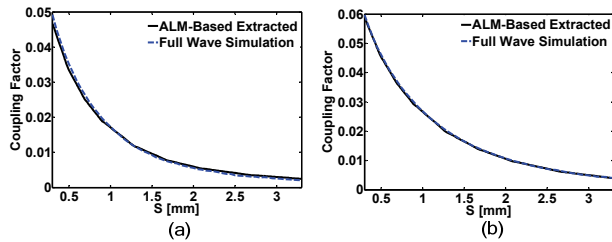


Fig. 10. ALM-based extracted coupling curves and full wave simulation, (a)  $h = 0.75$  mm cut of Fig. 8(a), and (b)  $h = 1.27$  mm cut of Fig. 8(a).

FVU is proportional to the mean square error. As the model accuracy increases, the FVU approaches zero and CC approaches one. To consider the accuracy of the extracted surfaces two different cuts of Fig. 8(a) as an example are considered ( $h = 0.75$  mm and  $h = 1.27$  mm). These two cuts are shown in Fig. 10 by solid lines while the corresponding full-wave-based extracted data are demonstrated by dashed lines. As it is seen they are in good agreement. Computing FVU and CC results in  $FVU = 0.0039$  and  $CC = 0.9999$  for Fig. 10(a) and  $FVU = 0.0005$  and  $CC = 0.9999$  for Fig. 10(b). These

values show the modeling accuracy of the proposed approach. Accuracy of the extracted surfaces is validated again in the next section by a filter design example.

### 4. Filter Design

In order to show the accuracy of the extracted coupling and external Q surfaces, a four pole Chebychev bandpass filter was designed and fabricated. Required physical parameters of the structure were related to the coupling and external Q of the filter using ALM-based extracted surfaces. Center frequency and the fractional bandwidth of the filter are 1.765 GHz and 5% respectively. The coupling matrix and  $Q_{ext}$  are as follows.

$$M = \begin{bmatrix} 0 & 0.0448 & 0 & 0 \\ 0.0448 & 0 & 0.0346 & 0 \\ 0 & 0.0346 & 0 & 0.0448 \\ 0 & 0 & 0.0448 & 0 \end{bmatrix} \quad (16)$$

$$Q_{ext} = 19.2$$

Physical structure of the filter is shown in Fig. 11. Dimensions of the resonators are  $W = 0.7$  mm,  $g = 0.6$  mm,  $L = 5.6$  mm and  $d = 0.3$  mm (Fig. 7). The filter is fabricated on a substrate of Rogers, TMM10i, with a relative permittivity of 9.8. In order to satisfy the center frequency of the filter, substrate thickness is selected equal to 1.27 mm. Considering the physical structure of the filter, the first and the last two resonators are mixed coupled while the second and the third resonators are magnetically coupled. Therefore, the spacing between the mixed coupled resonators, i.e.,  $S_{12}$  and  $S_{34}$  (Fig. 11) is determined easily using  $h = 1.27$  mm cut of Fig. 8(a) which is shown in Fig. 10(b) with the solid line. This curve results in  $S_{12} = S_{34} = 0.55$  mm. In the same way, considering  $h = 1.27$  mm cut of Fig. 8(b) results in  $S_{23} = 0.5$  mm. Using ALM-based extracted  $Q_{ext}$  surfaces, for  $Q_{ext} = 19.2$  various triplets of  $(L_f, W_f, D_f)$  are calculated. Among these different choices,  $L_f, W_f,$  and  $D_f$  were selected 5 mm, 0.4 mm, and 1.6 mm respectively. The simulated and measured responses of the filter are demonstrated in Fig. 12. As it is seen they are in good agreement.

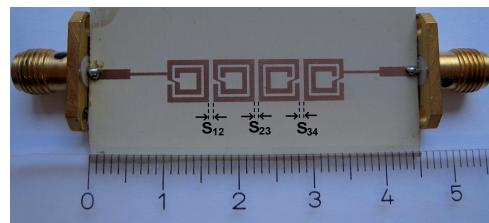


Fig. 11. Fabricated SR filter.

In order to show the miniaturization degree of the SR filter in comparison with an ordinary open loop resonator one, a SOLR filter with the same degree and nearly the same electrical characteristics (center frequency equal to 1.64 GHz and fractional bandwidth equal to 4%) was de-

signed and fabricated on the same substrate. The fabricated filter and responses are shown in Fig. 13. The total active area of this filter (excluding feed lines) is 4.97 cm<sup>2</sup> while this area is 1.34 cm<sup>2</sup> for the SR one (Fig. 11). It shows more than 70% of miniaturization for the SR filter in comparison with the SOLR one.

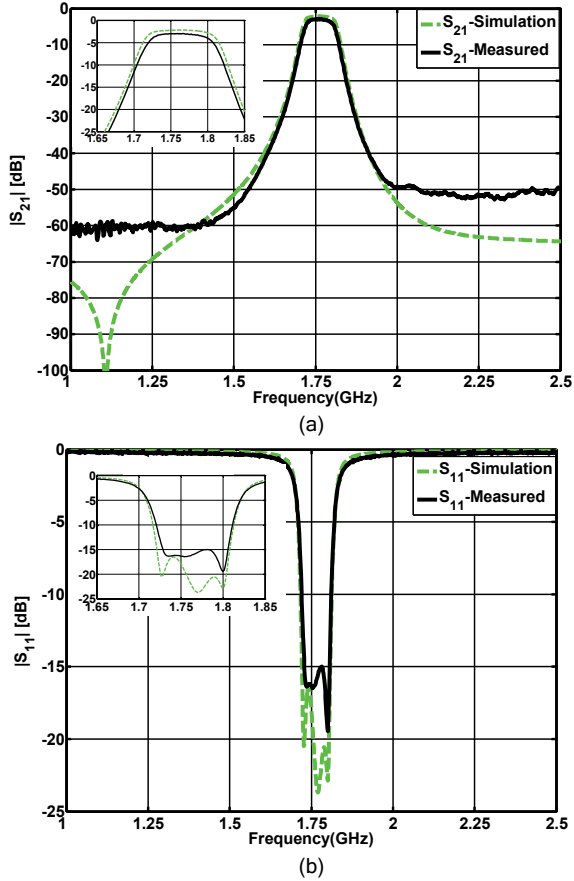
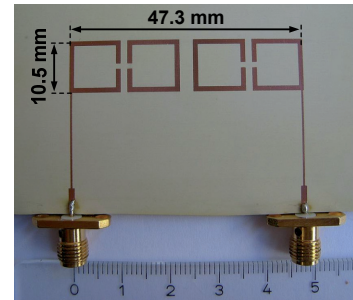


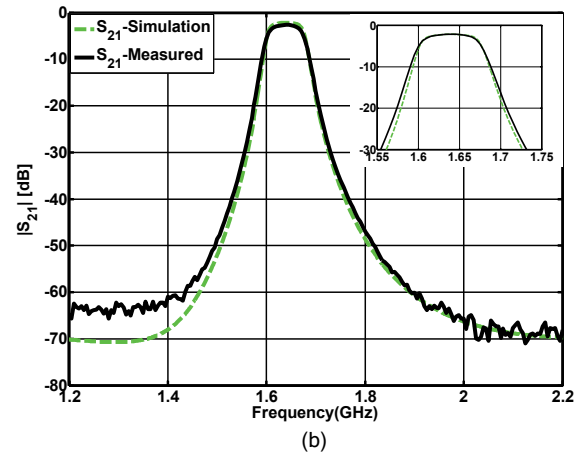
Fig. 12. Measured and simulated response of the spiral filter, (a) amplitude of the  $S_{21}$  (in-band response is shown inset) and (b) amplitude of the  $S_{11}$  (in-band response is shown inset).

Design process of the SOLR filter is similar to the explained procedure of the SR filter design. In this regard, we implemented ALM to model coupling and external quality factor. Modeling parameters of the external quality factor were feed line length, feed line width and feed line position. Coupling factor was also modeled for two different coupling structures, i.e., electric and magnetic coupling. In this modeling, three different parameters were considered which are spacing between resonators, resonator length, and substrate permittivity. Successful ALM-based modeled coupling and external quality factor in the case of SOLRs and SRs shows the ability of ALM in modeling different resonant structures. Considering three different parameters in coupling factor modeling of the coupled SOLRs, in comparison with two ones for the coupled SRs, validates the capability of ALM in extending the number of modeling parameters. These surfaces provide a fast and useful tool for SOLR filter design in a relatively wide

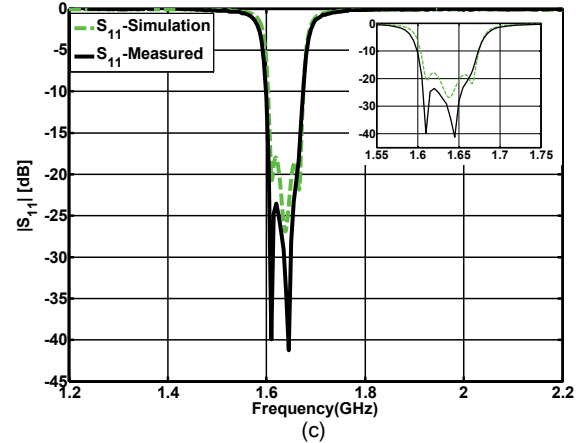
variation range of required filter characteristics such as center frequency and bandwidth. Samples of extracted ALM-based coupling factor surfaces for the electrically coupled SOLRs have been represented in Fig. 14.



(a)



(b)



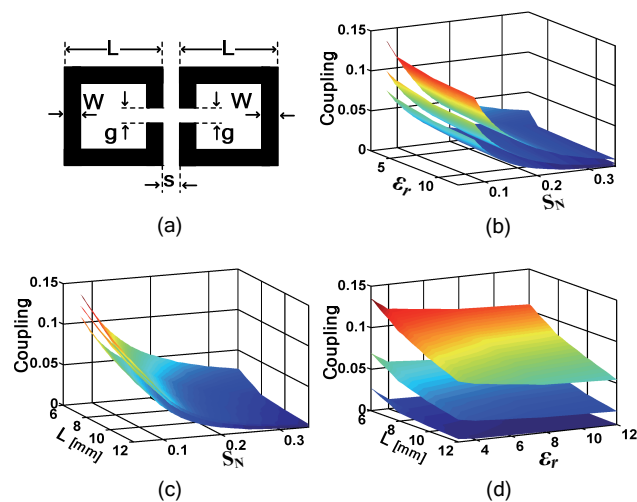
(c)

Fig. 13. (a) Fabricated square open loop resonator filter, (b) amplitude of the  $S_{21}$  (in-band response is shown inset), and (c) amplitude of the  $S_{11}$  (in-band response is shown inset).

## 5. Conclusions

In this paper, a novel approach based on ALM has been proposed to model coupling and external quality factor of SRs. Spacing between resonators and substrate height were the coupling factor modeling parameters, and feed line length, feed line width, and feed line position were the external quality factor modeling parameters. The

modeling was carried out within a wide range of modeling parameters surprisingly fast and accurate. Accuracy of the extracted surfaces was verified using two different error measures. Using the ALM-based-extracted coupling and external quality factor surfaces one four pole Chebyshev bandpass filter was designed and fabricated. Good agreement between the measured and full wave simulated response of the filter validated the accuracy of the extracted surfaces again. The same process, using ALM-based-extracted coupling and external quality factor surfaces, was carried out to design a SOLR filter. Good agreement between the measured and full wave simulated response of the filter shows the accuracy of the method and its generality in modeling different resonant structures. Comparison between these two filters determined more than 70% of area reduction for SR filters. The proposed modeling approach for coupling and external quality factor is general and can be used for other kinds of coupling configurations, other resonators or other feeding structures with the same degree of simplicity. It is also possible to consider more than three parameters in the proposed modeling approach simply, if we add initial required data of the new parameters to the previous ones.



**Fig. 14.** (a) Electrically coupled SOLRs. Extracted coupling surfaces for the electrically coupled SOLRs shown in Fig. (14-a), (b)  $L = 6$  mm (top),  $L = 9$  mm (middle),  $L = 12$  mm (bottom), (c)  $\epsilon_r = 3$  (top),  $\epsilon_r = 4$  (middle)  $\epsilon_r = 12$  (bottom), and (d)  $S_N = 0.08$  (top),  $S_N = 0.16$  (middle),  $S_N = 0.35$  (bottom).  $S_N$  is the normalized spacing between resonators ( $S_N = S/L$ ).

## References

- [1] MIRAFTAB, V., MANSOUR, R. R. Computer-aided tuning of microwave filters using fuzzy logic. *IEEE Transact. on Microwave Theory and Techniques*, 2002, vol. 50, no. 12, p. 2781 - 2788.
- [2] MIRAFTAB, V., MANSOUR, R. R. A robust fuzzy-logic technique for computer-aided diagnosis of microwave filters. *IEEE Transactions on Microwave Theory and Techniques*, 2004, no. 1, vol. 52, p. 450 - 456.
- [3] TAYARANI, M., KAMI, Y. Qualitative analysis in engineering electromagnetic; an application to general transmission lines. *IEIEC Transactions on Electronics*, 2001, vol. E84-C, no. 3, p. 364 - 375.
- [4] GUNEY, K., SARIKAYA, N. Resonant frequency calculation for circular microstrip antennas with a dielectric cover using adaptive network-based fuzzy inference system optimized by various algorithms. *Progress in Electromagnetics Research, PIER* 72, 2007, p. 279 - 306.
- [5] GUNEY, K., SARIKAYA, N. Concurrent neuro-fuzzy systems for resonant frequency computation of rectangular, circular and triangular microstrip antennas. *Progress in Electromagnetics Research, PIER* 84, 2008, p. 253 - 277.
- [6] OSTADZADEH, S. R., SOLEIMANI, M., TAYARANI, M. A fuzzy model for computing input impedance of two coupled dipole antennas in the echelon form. *Progress in Electromagnetics Research, PIER* 78, 2008, p. 265 - 283.
- [7] OSTADZADEH, S. R., SOLEIMANI, M., TAYARANI, M. A fuzzy model for computing back-scattering response from linearly loaded dipole antenna in the frequency domain. *Progress in Electromagnetics Research, PIER* 86, 2008, 229 - 242.
- [8] KABIR, H., WANG, Y., YU, M., ZHANG, Q.-J. High-dimensional neural-network technique and applications to microwave filter modelling. *IEEE Transactions on Microwave Theory and Techniques*, 2010, vol. 58, no.1, p. 145 - 156.
- [9] TAKAGI, T., SUGENO, M. Fuzzy identification of systems and its application to modeling and control. *IEEE Transactions on Systems, Man and Cybernetics*, 1985, vol. SMC. 15, no. 1, p. 116 - 132.
- [10] TAKAGI, T., SUGENO, M. A fuzzy logic approach to qualitative modelling. *IEEE Transactions on Fuzzy Systems*, 1993, vol. 1, no. 1, p. 1282 - 1285.
- [11] SHOURAKI, S. B., HONDA, N. Recursive fuzzy modeling based on fuzzy interpolation. *Journal of Advanced Computational Intelligence*, 1999, vol. 3, no. 2, p. 114 - 125.
- [12] SHOURAKI, S. B., HONDA, N. Fuzzy interpretation of human intelligence. *International Journal of Uncertainty, Fuzziness and Knowledge-based Systems*, 1999, vol. 7, no. 4, p. 407 - 414.
- [13] HONG, J. S., LANCASTER, M. J. Coupling of microstrip square open-loop resonators for cross-coupled planar microwave filters. *IEEE Transactions on Microwave Theory and Techniques*, 1996, vol. 44, no.12, p. 2099 - 2109.
- [14] RIZZI, P. A. *Microwave Engineering: Passive Circuits*. Prentice-Hall, 1988.
- [15] HONG, J. S., LANCASTER, M. J. Canonical microstrip filter using square open-loop resonators. *IET Electronics Letters*, 1995, vol. 31, no. 23, p. 2020 - 2022.
- [16] CHAIMOOL, S., KERDSUMANG, S., AKKARAEKTHALIN, P. A novel microstrip bandpass filter using triangular open-loop resonators. In *Proceedings of the 9<sup>th</sup> IEEE Asia Pacific Conference on Communication*. Penang (Malaysia), 2003, p. 788 - 791.
- [17] ROMANI, I. N. A., SOARES, J. M. A., ABDALLA, H. Compact microstrip bandpass filter with enhanced stopband performance. In *Proceedings of the 12<sup>th</sup> IEEE International Microwave and Optoelectronics Conference*. Salvador (Brazil), 2007, p. 950 - 953.
- [18] MAO, R. J., TANG, X. H., WANG, L., DU, G. H. Miniaturized hexagonal stepped-impedance resonators and their applications to filters. *IEEE Transactions on Microwave Theory and Techniques*, 2008, vol. 56, no. 2, p. 440 - 448.

## About Authors ...

**Payman REZAEI** was born in Kermanshah, Iran, in 1980. He received the B.Sc. and M.Sc. degrees both in Electrical Engineering from Iran University of Science and Technology (IUST), Tehran, Iran in 2002 and 2005 respectively and is currently working toward the Ph.D. degree in Electrical Engineering. His research interests include soft computing techniques in complicated electromagnetic problems, microwave linear and nonlinear circuit design, microwave measurement techniques and metamaterial structures.

**Majid TAYARANI** was born in Tehran, Iran, in 1962. He received the B.Sc. degree from Iran University of Science and Technology, Tehran, Iran, in 1988, the M.Sc. degree from Sharif University of Technology, Tehran, Iran in 1992, and the Ph.D. degree in communication and systems from the University of Electro-Communications, Tokyo, Japan, in 2001. From 1990 to 1992, he was a Researcher with the Iran Telecommunication Center, where he was involved with nonlinear microwave circuits. Since 1992, he has been a member of the faculty with the Department of Electrical Engineering, Iran University of Science and Technology, Tehran, Iran, where he is currently an Assistant Professor. His research interests are qualitative methods in engineering electromagnetic, electromagnetic compatibility (EMC) theory, computation and measurement techniques, microwave and millimeter-wave linear and nonlinear circuit design, microwave measurement techniques, and noise analysis in microwave signal sources.

**Reinhard KNÖCHEL** (IEEE Fellow) received the Dipl.-Ing. degree in Electrical Engineering in 1975 and the Dr.-Ing. degree in 1980 from the Technical University, Braunschweig, Germany. From 1980 to 1986, he was a Principal Scientist at the Philips Research Laboratory, Hamburg, Germany. In 1986, he joined the Technical University Hamburg-Harburg, where he was a Full Professor in microwave electronics until November 1993. Since December 1993, he has held the Chair in Microwave Engineering at the University of Kiel, Kiel, Germany, where he serves as Dean of the Department. His research interests include active and passive microwave components, ultrawideband technology, microwave measurement techniques, industrial microwave sensors, and radar. He has published more than 240 papers in reviewed journals and at scientific conferences. He was Guest Editor of the book *Sensors Update*, Vol.7 (Wiley-VCH), and the special issue on ultrawideband of the IEEE TRANSACTIONS ON MICROWAVE THEORY AND TECHNIQUES, vol. 54, April 2006. He has authored 39 patents. Dr. Knöchel is active in the IEEE. He serves on the TPRC of the IEEE Microwave Symposium (IMS) and is the Chair of the Technical Committee MTT-16 on Microwave Systems. He was the General Chairman of the German Microwave Conference 2008. He is a Fellow of the IEEE "for contributions to microwave systems and sensors for industrial process control." He is a member of URSI Commission A, and a member of the German Institute of Electrical Engineers VDE-ITG. He was recipient of the VDE best-paper award 1978, the European Microwave Prize 1980, and the TSH-Technology Transfer Award in 2003.